

Icephobic Gradient Polymer Coatings Coupled with Electromechanical De-icing Systems: A Promising Ice Repellent Hybrid System

Gabriel Hernández Rodríguez, Giulia Gastaldo, Luca Stendardo, Younes Rafik, Jason Pothin, Marc Budinger, Carlo Antonini, Valérie Pommier-Budinger, and Anna Maria Coclite*

Icephobic materials and systems are highly desired in regions and seasons where daily life activities are hindered by the presence of ice. The combination of icephobic materials with active de-icing systems, known as hybrid systems, is a promising way to optimize efficiency in ice removal, while reducing power consumption. However, the development of hybrid systems is limited by their lifespan and the incompatibility of most icephobic materials with the operating mode of the active system. Here we present a hybrid system comprising a gradient polymer coating deposited with initiated chemical vapor deposition and a resonant piezoelectric de-icing system. The de-icing performance is evaluated in an icing wind tunnel, where the system is capable of detaching ice blocks in less than 1 s, regardless the ice type and covered area. An in-depth ice detachment study confirms that ice adhesion reduction is an intrinsic property of the coating, independent from external factors. The nanometric nature of the coating enables efficient operation of the resonant de-icing systems. The coating shows outstanding durability against the de-icing cycles, abrasion, water erosion, and delamination. The results showcase the hybrid systems potential in real-world applications to contrast icing.


1. Introduction

The development of materials and systems that successfully act against ice formation, accretion, and adhesion of ice would significantly impact daily life during cold seasons or in locations where low temperatures are a constant challenge. The demand for such materials or systems has increased in the past years,^[1,2] and materials with so-called icephobic properties have been developed to mitigate ice by inhibiting ice nucleation, delaying propagation, and/or significantly reducing ice adhesion.^[3–5] Icephobic materials, their properties, and the phenomena around them have been widely studied.^[6,7] Unfortunately, in most cases, the materials are unsuitable for industrial, large-scale applications and are only suitable for use in limited environmental conditions.^[8,9]

Studies indicate that icephobic materials are not a standalone solution for anti-icing or de-icing. To date, no icephobic material has been identified that can withstand harsh environmental conditions while maintaining its functionality. This has limited the

G. Hernández Rodríguez, A. M. Coclite
Institute of Solid State Physics
NAWI Graz
Graz University of Technology
Graz 8010, Austria
E-mail: anna.coclite@tugraz.at

G. Gastaldo, V. Pommier-Budinger
Fédération ENAC ISAE-SUPAERO ONERA
University of Toulouse
Toulouse 31400, France

 The ORCID identification number(s) for the author(s) of this article can be found under <https://doi.org/10.1002/adem.202401532>.

© 2024 The Author(s). Advanced Engineering Materials published by Wiley-VCH GmbH. This is an open access article under the terms of the Creative Commons Attribution-NonCommercial License, which permits use, distribution and reproduction in any medium, provided the original work is properly cited and is not used for commercial purposes.

DOI: 10.1002/adem.202401532

L. Stendardo, C. Antonini
Department of Materials Science
University of Milano-Bicocca
via R. Cozzi 55, Milano 20125, Italy

Y. Rafik, J. Pothin, M. Budinger
Institut Clement Ader
University of Toulouse
INSA
ISAE-SUPAERO
MINES ALBI
UPS
CNRS
Toulouse 31055, France

A. M. Coclite
University of Bari
via Amendola 173, Bari 70125, Italy

application of such coatings because once a single ice layer forms, ice accretes, thereby suppressing the surface icephobicity.^[2,9–11] As a solution, the construction of hybrid systems has been proposed; these systems consist of coupling icephobic coatings with active ice protection systems, such as electrothermal,^[12,13] pneumatic boots,^[14] shape-memory materials,^[15,16] and ultrasound or microwave technologies.^[17] Hybrid systems seem an appealing alternative to overcome the current performance limitations of anti-icing and de-icing systems operating individually.

Electrothermal de-icing systems have been widely investigated due to the simplicity of the concept: the principle consists of integrating electrical heating elements into the desired protected surface.^[2,11] However, one of the primary limitations is the substantial amount of electrical energy required for the operation. In some cases, achieving the melting temperature is insufficient and temperatures above 10 °C are required, which further increases the energy consumption,^[2,18] not to mention the problem of run-back ice, which may require operation with strongly energy-demanding full-evaporative systems. Electrothermal de-icing systems have been combined with icephobic coatings resulting in a reduction in power consumption. Fortin et al.^[19] reported that the power reduction on de-icing systems coupled with icephobic coatings depended on the type of ice accreted and whether the coating employed had hydrophobic or superhydrophobic properties. Antonini et al.^[20] used a Teflon coating on etched aluminum and reported a reduction of power up to 80% compared to the performances of the unpolished substrate. Additionally, a significant reduction of runback ice was observed in the presence of coatings. As discussed by Huang et al.,^[2] the proper selection of the coating is crucial for achieving a power consumption reduction.

Electromechanical resonant de-icing systems represent a viable alternative to traditional ice protection methods for limiting the required power. They can use piezoelectric actuators which generate vibrations in the iced surface. The vibrations result in the generation of localized stresses, which ultimately lead to the failure and detachment of the ice. Due to the small vibrational amplitude, the structural fatigue to the surface is minimal to other mechanical de-icing strategies, such as electromechanical expulsive or electroimpulsive systems.^[18,21–24] In a comparative analysis conducted by Palanque et al.,^[25] the power consumption of two electromechanical de-icing architectures for the Airbus A320 was investigated. Findings indicate that these systems require between 1.5 and 2 kVA m⁻², significantly lower than the 26.5 kW m⁻² consumed by the thermal anti-icing systems commonly employed on commercial airliners.

The combination of electromechanical de-icing systems with an icephobic coating that reduces ice adhesion can further improve the system's effectiveness and efficiency. However, the critical issue is the coating's mechanical properties which can negatively affect the transmission of vibrations, specifically the loss modulus, which has an impact on damping, and the Young's modulus, which, if too low, makes the coating layer soft and prone to vibration absorption.^[2]

Previously, gradient polymeric coatings exhibiting a broad range of icephobic properties and extraordinary durability were presented.^[26] These nanometric coatings were formed and deposited via initiated chemical vapor deposition (iCVD), a one-step technique that does not require solvents and that has been

successfully adapted for the industrial scale.^[27,28] The gradient coating composition was gradually changed from the one of a organosilicon polymer to the one of a perfluoroacrylate polymer, namely, 2,4,6,8-tetraethenyl-2,4,6,8-tetramethylcyclotetrasiloxane (pV4D4) and 1*H*,1*H*,2*H*,2*H*-perfluorodecyl acrylate (PFDA), respectively. It was found that when the top section (pPFDA) thickness of the gradient structure increased, a systematic change in crystallographic orientation at the surface plane ensued, producing a discontinuity in the surface energy. The predominantly random-oriented structure at the surface leads to a systematic enhancement of the icephobic properties of the coating. In other words, the higher the surface energy discontinuity, the more effective the icephobic properties. This was particularly observed and quantified in the coating ability to reduce ice adhesion by an adhesive reduction factor (ARF) of at least 20 times.^[26] During the coating characterization via push test, a distinct fracture propagation mechanism was observed, indicative of a toughness-dominated detachment process. This mechanism is characterized by a low detaching force that is independent of the iced area.^[29–31] Consequently, these coatings possess an advantageous property, which is a low toughness at the ice/surface interface when compared to unpolished substrates.

Although hybrid systems represent a viable alternative to mitigate ice, existing icephobic coatings face limitations, these include a lack of mechanical durability, thermal stability, and chemical resistance, as well as the coating deposition technique, leading to incompatibility with large-scale industrial applications and current de-icing systems.^[1,2] In this study, the versatility of iCVD was leveraged to coat a range of substrates. Aluminum plates were coated and equipped with piezoelectric actuators to create a hybrid electromechanical de-icing system. The coating's nanometric nature did not introduce any damping that would have limited the vibration transmission, thereby highlighting the potential of iCVD coatings over traditional coatings and methods for the combination of passive ice protection systems with resonant electromechanical active systems. The system was tested in an icing wind tunnel (IWT) simulating atmospheric icing conditions and for the first time, a hybrid system composed of a nanometric polymeric coating showed promising de-icing performance. The action-responsive times were less than a second, and an outstanding resistance against the mechanical stresses after multiple icing/de-icing cycles was observed. The ice detachment mechanism in relatively large areas was characteristic of coated surfaces with fewer cohesive fractures. The final result was a full ice-block detachment with less energy than experiments with an uncoated plate.

As previously demonstrated,^[29] ice adhesion is influenced by experimental conditions such as temperature, relative humidity, cooling rate, and ice sample size and geometry. Therefore, an extended ice adhesion study is presented to validate that the ice adhesion reduction displayed by the gradient polymer surfaces, observed in the de-icing experiments in the IWT, is an intrinsic property of the material independent of external variables. In the end, gradient polymers manufactured via iCVD demonstrated not only outstanding icephobic properties but also proved to be viable candidates for combination with resonant electromechanical de-icing systems, resulting in hybrid systems exhibiting high performance and durability in outdoor conditions.

2. Results and Discussion

To understand the contribution of the gradient polymer surfaces in the detachment process when coupled with the electromechanical de-icing system, an extended ice adhesion study is presented. As discussed by Stendardo et al.,^[29] the ice adhesion is influenced by experimental conditions such as temperature, relative humidity, cooling rate, and ice sample size and geometry. A series of gradient polymer coatings with different top section thicknesses, 100, 200, and 300 nm, was deposited over silicon substrates via iCVD. As a preliminary experiment, the ice adhesion of the gradient coating series was tested to evaluate the effect of surface temperature and cooling rate. **Figure 1a** shows the ice adhesion force of the gradient polymer coatings as a function of the temperature with the “fast” cooling method. When comparing all temperatures, no effect was observed in the ice adhesion force values, which stayed constant. However, at each temperature, the following trend was observed: as the top section thickness increased, the ice adhesion force systematically decreased, with Grad300 displaying the lowest force. This experimental case evidenced that the ice detachment mechanisms exhibited by the gradient polymer coatings were not temperature-dependent and that the ice adhesion systematically decreased with an increment of the coating thickness. As demonstrated previously,^[26] the only difference between the three gradient coatings is the randomness of the crystallites at the surface, which increases for thicker coatings.

Figure 1b shows the adhesion force results with the “slow” cooling method, which resulted in two different outcomes: a global increase in ice adhesion on each sample, compared to the “fast” cooling method, and a systematic reduction in ice adhesion as the temperature decreased. In accordance with previous observations, the ice adhesion force systematically decreased, as the top section thickness increased. At each temperature, Grad300 remained the coating with the lowest adhesion force. This experimental case demonstrated that the icephobic properties prevailed over the temperature in the testing conditions, and the ice detachment mechanism remained the same. This was not only visible in the tendency at “fast” cooling rates but was also reproduced at “slow” cooling rates. In a previous contribution,^[26] it was demonstrated that the main difference between the gradient coatings resides in the crystal orientation; hence, this

demonstrates that the superior performance of Grad300 is due to its characteristic crystallinity. Finally, this study confirms the ice adhesion reduction ability as an intrinsic icephobic property of the gradient polymer coatings and possibly originated from the difference in the crystal orientation, as it is the only different attribute among them. Figure 1c compares the two cooling mechanisms. Although the exact reason behind the global force increment for the “slow” cooling method is still uncertain, we speculate that it can be related to the ice mechanical properties because ice is more brittle when water cooling and freezing occur rapidly.

As Grad300 was the coating with the strongest icephobic properties regarding the lowest adhesion force, it was chosen for further experiments on aluminum. The surface properties of the gradient polymer coatings were successfully transferred to the aluminum surface as the water contact angle (WCA) analysis and ice adhesion assessment confirmed. **Figure 2a** shows the WCA analysis of the unpolished aluminum (as received from the manufacturer), polished, and coated. The polished aluminum sample showed lower static WCA compared to the unpolished one, with a difference of 20°. This difference in wettability is attributed to the roughness of the unpolished aluminum, approximately $S_p = 0.56 \mu\text{m}$, which comes from the contiguous unidirectional brushing in the surface. The polished aluminum substrates exhibited a strong hydrophilic behavior, likely due to the enhanced contact area of the water with the surface, which was a consequence of the elimination of the topographical features. In contrast, the unpolished substrate displayed a weaker hydrophilic behavior, likely due to the presence of brushing, which hinder the mobility of the drop in the surface.

By using iCVD, conformal coatings are formed,^[32,33] i.e., all the features existing at the surface are uniformly covered by the coating; this is shown in the optical micrographs in Figure 2b. In the polished coated surface, there were no features influencing the interaction of the coating with water; hence, the typical hydrophobic behavior of Grad300 was observed.^[26] The unpolished coated sample exhibited weaker hydrophobicity than the polished sample. In this case, the roughness promoted the pinning effect more than enhancing the wetting, as indicated by the stronger hysteresis and lower WCA values. Figure 2c compares the ARF for the samples with Grad300 and without coating. The coating successfully decreased the ice adhesion on the unpolished

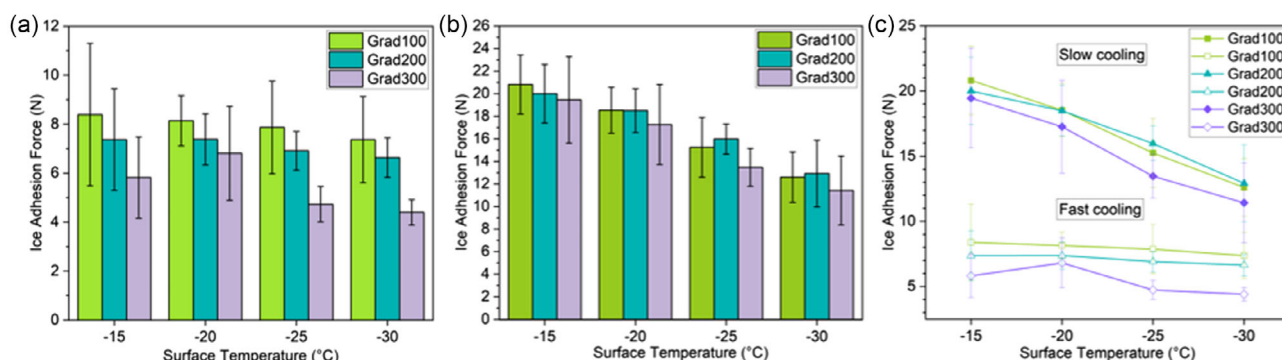


Figure 1. Ice adhesion force exhibited by the gradient polymer coatings as a function of temperature with a) “fast” cooling method and b) slow cooling method. c) Ice adhesion force comparison of both cooling methods.

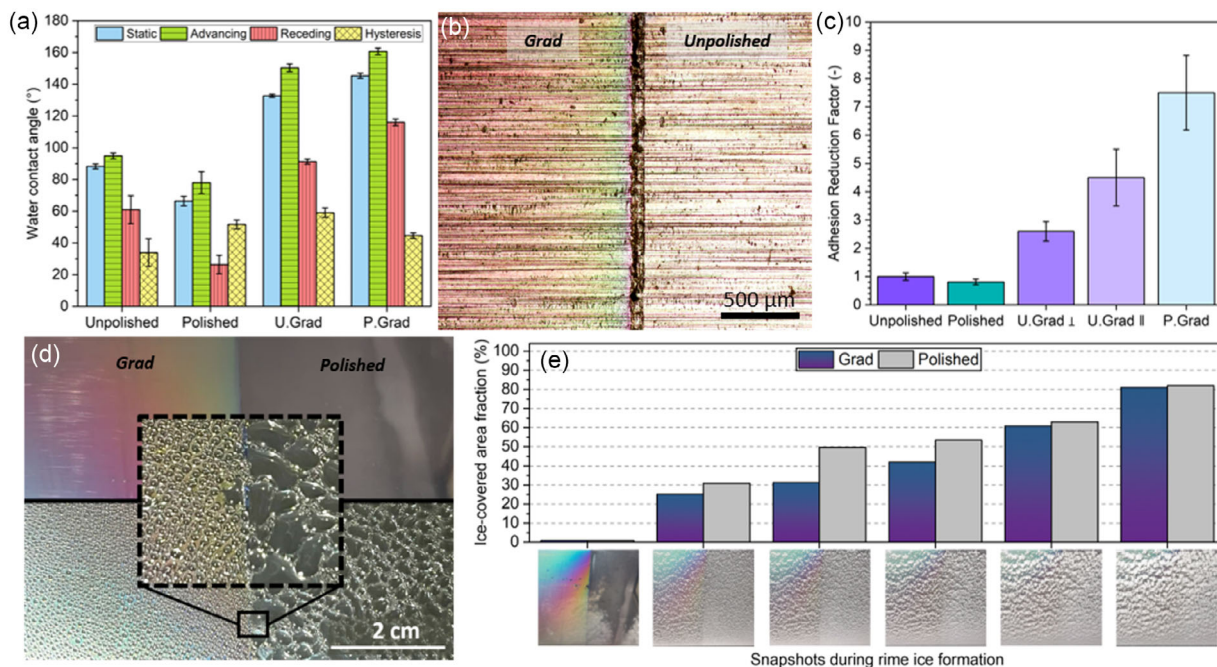


Figure 2. a) WCA analysis of the aluminum noncoated and Grad300-coated samples. b) Microscope image comparing the appearance of unpolished aluminum with and without coating. The brushing causing roughness can be distinguished with the bare eye and was conformally coated with iCVD. c) Ice adhesion reduction comparison of unpolished and polished uncoated aluminum samples with unpolished and polished Grad300-coated samples. The unpolished sample with parallel brushing (||) and perpendicular brushing (⊥) displayed differences due to the interlocking effect. d) A close-up image at the boundary of the Grad300-coated part on the half-coated polished plate allows for a comparison of the wettability observed along the plate ($300 \times 70 \times 1 \text{ mm}^3$) on both parts of the plate. To achieve a partial coating with iCVD, a mask covering the noncoated area was used during the deposition. e) The graph shows a comparison of the area coverage at different moments during the rime ice formation over the half-coated plate (see the full sequence in the Video S1, Supporting Information).

surface, with a reduction factor of at least 2.6 times, whereas on the polished surface, the reduction was 7.5 times. In the unpolished coated sample, an anisotropic effect due to the unidirectional brushing was observed. Two experiments were performed: one with the pushing force direction perpendicular (⊥) and the other parallel (||) to the direction of the brushing. In the perpendicular configuration, the reduction factor was found to be lower than in the parallel configuration, i.e., 2.6 and 4.5, respectively. This was attributed to physical ice interlocking, i.e., the water penetrates within the brushing and, when it freezes, it creates anchor points promoting ice adhesion. Although the parallel configuration favored the ice detachment reducing 4.5 times the ice adhesion, there was still a significant difference compared to the polished coated, whose reduction was 7.5 times smaller. While the roughness effect on ice adhesion has been previously discussed,^[34–36] these experiments provide a more comprehensive understanding of how ice adhesion is affected by the roughness of an icephobic surface. To avoid roughness influences and to characterize the pure icephobic performance of the gradient polymer coating, the aluminum samples were polished for IWT testing.

Ice accretion was tested in coated and noncoated aluminum plates fixed in the IWT chamber as shown in Figure S3, Supporting Information. Prior to ice accretion tests, the wettability of the plates was observed at room temperature by spraying water through the IWT nozzles. Due to the strong pinning effect

and hydrophobic character of the coating, drops maintained uniform size and distribution with clear dry zones separating them, analogous to the previous observations reported in our previous contribution.^[26] At a certain drop volume, the pinning effect was overcome and drops rolled off the surface, drying their way (Video S1, Supporting Information). In the noncoated area, drops covered the entire surface, forming a quasicontinuous water layer. This phenomenon was clearly observed at the boundary of the coated/noncoated part, located in the middle of the half-coated plate, as shown in Figure 2d. Despite the noticeable difference in the wettability, the formation of several types of ice in the icing wind tunnel (glaze, rime, and mixed) was not affected resulting in homogeneous ice blocks. Only a slight difference was observed during the formation of rime ice when the plate was tilted 45° . Figure 2e shows the evolution of the ice-covered area observed at the boundary of the coated and noncoated part; this was obtained by analyzing snapshots during the process. The ice-covered area in the coated part was smaller than in the noncoated during the early part of the experiment, but eventually, the accreted rime ice covered both areas equally. The experiment was concluded when the ice accreted reached a thickness of 30 mm. The limited icephobic performance that Grad300 displayed as a purely passive system was in line with expectations, as at some point ice will start to form on any surface, leading to ice accretion. Nevertheless, the point of IWT tests is to form ice in challenging conditions ($T_{\text{chamber}} = -5^\circ\text{C}$, $v_{\text{wind}} = 20 \text{ m s}^{-1}$, $\text{MVD} = 50 \mu\text{m}$,

LWC between 1 and 10 g m⁻³) similar to those in nature and assess the effective de-icing in combination with an active system.

As such, the aluminum plates were coupled with an electro-mechanical de-icing system to assess their compatibility and ice-phobic performance. On the back of the aluminum plates, five piezoelectric actuators were glued in the configuration shown in **Figure 3a**. This specific configuration was designed to excite the plate in two specific resonant modes: the second extensional mode and the second in-plane flexural mode. A detailed study on resonant modes and fracture propagation mechanisms has been published by Gastaldo et al.^[24] In **Figure 3b**, the polished uncoated plate equipped with the electromechanical de-icing system was placed in the IWT where ice accreted until the surface was covered by a uniform block of glaze ice, having a thickness of ≈3 mm. The electromechanical system was then activated, exciting the plate at its second extensional mode, with a frequency around 13 kHz. With this mode, the displacement is mostly in the in-plane direction. This is expected to induce high stresses at specific sites in the ice block producing cracks and eventual detachment from the aluminum surface.

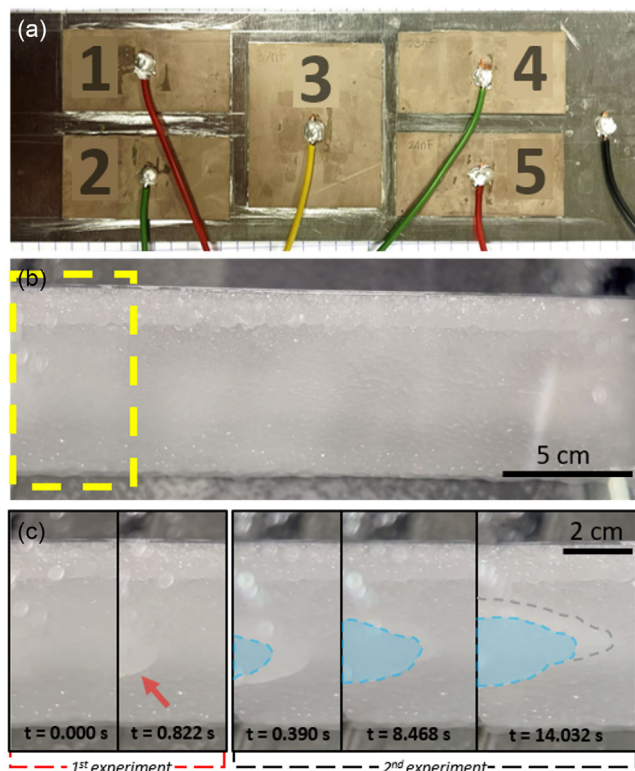


Figure 3. a) Configuration of the piezoelectric actuators on the back side of the aluminum plates. b) Ice accreted in the IWT over aluminum plates (300 × 70 × 1 mm³). The dashed area indicates the area in which a crack is formed and propagated during the excitation. c) During the first test, the formation of the crack occurred in less than 1 s after the start of the excitation. During the second test, the crack propagated adhesively (i.e., at the interface between the ice layer and the plate). The marked zones correspond to total crack propagation area. The dashed gray line is the maximum area achieved (see the full sequence in the Video S2, Supporting Information).

Noncoated plates were used as references. During the tests with the noncoated plate, only cracks were formed without achieving complete detachment. In the first test, the reference plate was excited for 10 s at 250 Vpk. A crack appeared on the left side of the ice block almost instantly when the piezoelectric actuators were activated ($t = 0.8$ s), as shown in **Figure 3c**. Although the opaque color near the crack indicated a localized detachment, the crack did not propagate during or after the excitation. The ice block was not affected and remained adhered to the plate. In the second test, the plate was excited for 10 s with 13 kHz and 200 V, in extensional resonant mode. The second excitation did not generate new cracks; however, it promoted the propagation of the existing one toward the center of the plate (**Figure 3c**). The crack propagated continuously during the excitation increasing the opaque area in the ice, and it stopped with an approximated length of 53 mm when the excitation ended.

The half-coated and fully coated plates were tested under the same conditions as the reference. The half-coated plate (**Figure 4a**) showed explicitly how the presence of the Grad300 coating significantly improved the de-icing performance of the electromechanical system. **Figure 4b** shows the experiment in which a continuous glaze ice block covers homogeneously the coated and noncoated part of the plate. The piezoelectric actuators were excited for 10 s around 13 kHz and at 200 Vpk+, again with the second extensional resonant mode. After only 0.1 s, several cracks originated at the left side of the plate and propagated along the entire coated area. At 1.5 s, a big ice piece detached from the coated area, while the cracks propagated to the noncoated area. It took 4.8 s to fully clear the ice from the coated area. In contrast, the ice continued being firmly adhered to the noncoated area, despite the cohesive cracks generated in the ice block during excitation. The test on the half-coated plate demonstrated the beneficial impact of the Grad300 coating on the de-icing process, specifically in relation to the second extensional mode. With similar results, a second type of mode, specifically the second in-plane flexural mode, was then tested. In this mode, the movement is primarily in the in-plane direction; however, rather than the plate merely extending longitudinally (as in the second extensional mode), it undergoes in-plane bending.

The same experiment was performed with two separated blocks of mixed ice in each area, as shown in **Figure 4c**. The piezoelectric actuators were excited for 10 s at 250 Vpk+ and around 7 kHz, corresponding to the second in-plane flexural mode. At only 0.1 s of excitation, a sequential crack formation, propagation, and ice detachment occurred almost simultaneously on the top-left side of the coated area. This was critical and triggered the full detachment of the rest of the ice block. Hence, in less than 1 s (0.2 s), the coated area was fully clear of ice. In the noncoated part, the ice block remained tightly adhered to the substrate during the whole experiment, and no evidence of cracking or adhesive propagation was observed. The same de-icing performance was observed with glaze ice blocks. The de-icing process observed suggested that the detachment occurred by a combination of cohesive and adhesive fractures.^[18] The ice fracture started as a cohesive fracture and then propagated adhesively until the ice detached. The exclusive detachment observed on the coated area revealed that the presence of the coating was a crucial element in the detachment process, thus aiding the electromechanical system.

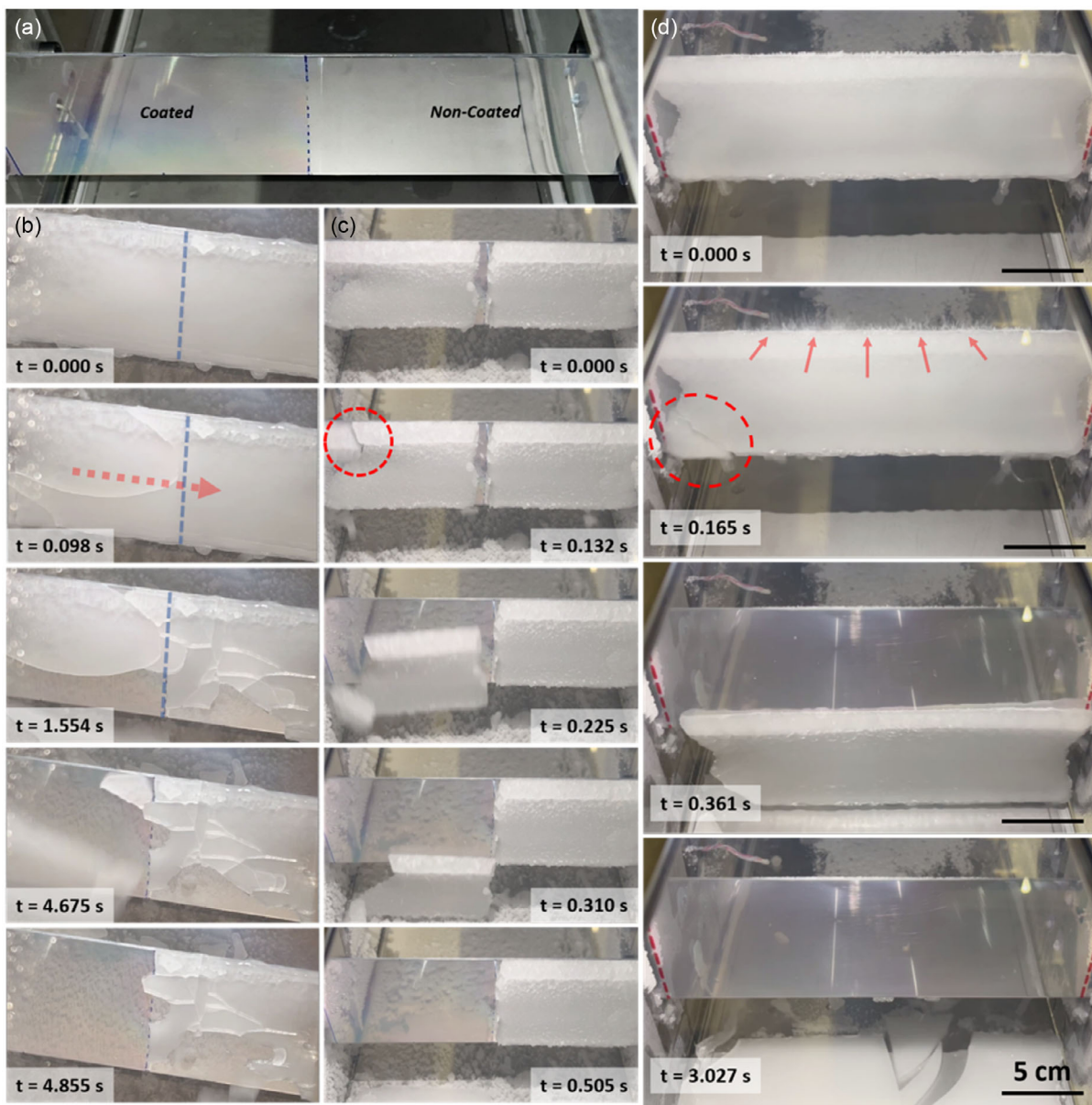


Figure 4. a) Half-coated plate inside the IWT before ice accretes to form an ice block. The iCVD coatings do not interfere with the substrate properties, it can be seen that the reflectiveness of the polished plate was preserved when coated with Grad300, and only a subtle rainbow color hue distinguishes the coated from the noncoated area. b) Sequential snapshots of the half-coated plate with a continuous glaze ice block during excitation. When the plate was excited, multiple cracks appeared on the coated area that propagated toward the noncoated area (dashed arrow). After 4 s, the coated area was clear of ice, whereas the ice remained adhered in the noncoated area. c) Sequential snapshots of the half-coated plate excitation with two separated blocks of mixed glaze and rime ice. When the plate was excited, a crack formed and propagated detaching a small piece of ice (dashed circle), followed by the detachment of the rest of the block in one piece in less than 1 s. d) Sequential snapshots of the fully coated plate excitation with a continuous glaze ice block. When the plate was excited, a crack formed and propagated detaching a small piece of ice (dashed circle), followed by the detachment of the rest of the block in one piece in less than 1 s. The detachment mechanism confirmed the low-interfacial toughness property of gradient polymer coatings (see the full sequence in the Video S3–S5, Supporting Information).

Figure 4d shows the experiment performed on the fully coated plate. Similar to previous experiments, once the surface of the plate was covered with a homogeneous mixed ice block, the piezoelectric actuators were activated for 10 s at 6.8 kHz and at 250 Vpk+. At 0.1 s of excitation, the vibrations produced a burst of ice crystals formed along the top of the ice block. Simultaneously,

the formation and propagation of a minor crack occurred at the bottom-left corner of the ice block, followed by a full adhesive detachment of the ice block in one piece. At only 0.3 s of excitation, the plate surface was completely ice-free.

Notably, the gradient polymer coating resisted multiple ice detachment cycles. The ice was accreted on each plate at least

10 times, and no signs of scratches, delamination, degradation, or decrease in effectiveness were observed. The cohesive and adhesive fractures were identified to occur in the same time scale, and in less than half of a second, the ice block was detached. No difference in the detachment mechanisms was observed between the small ice block (70 cm²) and a large ice block (140 cm²), proving the critical length is below the characteristic lengths of the ice blocks investigated in this study. Therefore, the fracture mechanism is always the same, independently of the area. These results are coherent with the toughness-dominated detachment mechanism previously associated with gradient polymer coatings observed in even smaller areas.^[26,29,31]

A key element behind the efficient performance of this system lies in the thickness of the coating. The nanometric nature of thickness plays an advantageous role in vibrational systems because the stresses generated by the actuators are fully delivered to the ice and are not dampened by the coating. This is not possible for soft coatings that potentially reduce the vibrations, compromising the de-icing effectiveness. Furthermore, no signs of wear were detected after several excitations. For the first time, iCVD was used to build a hybrid ice protection system demonstrating the versatility and compatibility of the technique with electromechanical de-icing systems. This system demonstrated quite promising results of high relevance to industrial applications.

3. Conclusion

Gradient polymer coatings deposited by iCVD possess intrinsic icephobic properties, proven to be temperature and ice type independent in different conditions. In this study, the icephobic performance was presented in a broad range of parameters allowing for a proper conceptualization of the material. Based on the best icephobic performance using a push test on silicon substrate, Grad300, where the upper polymer layer has a thickness of 300 nm, was selected to coat a series of aluminum plates. WCA analysis and ice detachment experiments demonstrated that icephobic properties can be easily transferred to aluminum using iCVD.

For the first time, iCVD was used to build a hybrid ice protection system by integrating gradient polymer coatings with piezoelectric actuators. The system was tested in the IWT and demonstrated highly effective de-icing performance independent of the iced area. The system is a practical alternative for ice mitigation due to its simplicity, minimal excitation, and fast response. Furthermore, the coating demonstrated remarkable resistance to scratches and delamination after numerous detachment cycles.

To conclude, we presented a comprehensive case study on the viability of gradient polymer coatings for ice-repellent functions. Further studies on the energy consumption and optimization are required to improve the limitations of the current technology. Additional evaluation in the IWT would provide a more robust understanding of the practical applications of this system with different icing conditions and ice thicknesses in real-world scenarios.

4. Experimental Section

Materials and Deposition Process: A series of gradient polymers with different properties were synthesized and deposited using a custom-made iCVD reactor with a standard configuration described elsewhere.^[28]

Di-*tert*-butyl peroxide (TBPO), purchased from Sigma–Aldrich, was used as an initiator with no further purification. V4D4 and PFDA were both purchased from Sigma–Aldrich and used as monomers without further purification. The iCVD reactor was operated in a continuous flow mode. The monomers V4D4 and PFDA were heated to ensure a constant flow into the reactor up to 80 and 95 °C, respectively. The flow rates were 1.0 ± 0.1 sccm for TBPO, 0.2 ± 0.05 sccm for V4D4, and 0.2 ± 0.05 sccm for PFDA. The flow rates were controlled using a needle valve. The reactor was operated at a pressure of 500 mTorr with a filament temperature of ≈200 °C and a substrate temperature of 40 °C. The formation of gradient structures followed previously reported procedures.^[26,37] A series of gradient polymers with top section thicknesses of 100, 200, and 300 nm, named Grad100, Grad200, and Grad300, respectively, were prepared on silicon substrates. The deposition thickness was followed in situ using a He–Ne laser. The selection of this coating was based on the icephobic properties displayed, mainly, the significant reduction of ice adhesion through a toughness-dominated detachment mechanism.^[26] The coatings were first deposited on silicon substrates for preliminary ice adhesion push tests. Silicon was chosen as a base material to eliminate any topological influence that might contribute to physical ice interlocking during the ice detachment experiments. It is shown later that the ice adhesion results can be greatly influenced by the surface roughness. It is therefore of high importance to minimize external effects on ice adhesion and to only account for the coating effect. After the first study on silicon substrates, aluminum (Al 6082) plates were homogeneously coated with the gradient polymer coating Grad300 for IWT tests. Three aluminum samples were studied: an uncoated plate, a half-coated plate, and a fully coated plate.

Characterization: The coating thickness was determined on silicon substrates via ellipsometry (M-2000 V ellipsometer from J.A Woolam Co.). Static, advancing, and receding WCA measurements were aluminum substrates using 10 μL of deionized water and advancing–receding rates of 0.4 μL s⁻¹. A Biolin Scientific's Optical Tensiometer Theta Flow was used. Atomic force microscopy (AFM) analysis was performed on aluminum substrates using a Nanosurf Easyscan 2 AFM with a scanning probe model PPP-NCLR-20 in tapping mode. An extended characterization of these coatings is found in our previous contribution.^[26]

Hybrid System Preparation: Coated and uncoated aluminum (Al 6082) plates of 300 × 70 × 1 mm³ were equipped with an array of five piezoelectric actuators glued to the rear surface using conductive adhesive. The piezoelectric actuators are soft piezoceramics made by PI in PIC255 material. The power electronics are from Amp-Line. The actuator control signal was generated in Matlab and transmitted to the power electronics via a National Instrument input/output card. All the devices are calibrated and allowed to ensure repeatability of the tests. The configuration of the piezoelectric components, detailed in Figure S1, Supporting Information, was based on simulations conducted on Ansys Workbench that provided the optimal arrangement to induce vibrations in both flexural and extensional modes.

Icing Wind Tunnel Tests: The aluminum plates were subject to testing in an icing wind tunnel, with their upper surface oriented perpendicular to the wind direction. Glaze, rime, and mixed ice were accreted on the plates. The formation of glaze ice, rime, and mixed ice followed specific parameters in the wind tunnel. Glaze ice was formed at a temperature of -4 °C with droplets of a media volumetric diameter (MVD) of 50 μm and liquid water content (LWC) between 1 and 10 g m⁻³ with an airspeed of 20 m s⁻¹. Water was injected for 60 s resulting in a very dense and homogeneous ice block with an average thickness of 3 mm. Rime ice was formed at a temperature of -10 °C, droplets of 50 μm MVD with an airspeed of 20 m s⁻¹. Water was injected for 60 s to ensure an ice thickness of ≈3 mm. Once ice had formed on the surface, a voltage sweep was performed to identify the natural frequencies of the iced-covered plates, and the plates were excited with a voltage ranging from 200 to 250 V around these frequencies. The de-icing tests were recorded with a digital camera from which snapshots were retrieved and analyzed with the software ImageJ.

Ice Adhesion Experiments: A custom-built setup, developed at the University of Milano-Bicocca and described elsewhere,^[29] was used to quantify the adhesion force on both substrates. A block of ice was formed by pouring distilled water into a cylindrical mold with an inner diameter of 8 mm, placed over the substrates, and frozen at -15, -20, -25, and

−30 °C. Two different cooling ramps were executed. In the “fast” method, the mold was filled with water once the testing temperature was reached, and then 15 min were waited before the experiment started. In the “slow” method, the mold was filled at −3 °C, and the temperature was reduced by 2 and 3 °C alternatively with 5 min between each reduction until the testing temperature was reached. Details regarding the cooling ramps can be found in the Figure S2, Supporting Information. A metallic rod coupled to a force gauge was used to push the mold at a constant velocity (0.01 mm s^{−1}) and to measure the force at which the ice was detached. To avoid the condensation of water vapor, the relative humidity was decreased through a continuous introduction of nitrogen into the chamber (ambient temperature $T_{amb} = 20$ °C, RH < 3%).

Received: June 28, 2024

Revised: August 29, 2024

Published online:

Supporting Information

Supporting Information is available from the Wiley Online Library or from the author.

Acknowledgements

This project has received funding from the European Union’s Horizon 2020 research and innovation program under the Marie Skłodowska-Curie grant agreement no. 956703 (SURFACE Smart surface design for efficient ice protection and control). Supported by TU Graz Open Access Publishing Fund.

Conflict of Interest

The authors declare no conflict of interest.

Author Contributions

Gabriel Hernández Rodríguez: Conceptualization (equal); Data curation (lead); Formal analysis (equal); Investigation (lead); Visualization (lead); Writing—original draft (lead); Writing—review and editing (supporting). **Giulia Gastaldo:** Conceptualization (equal); Data curation (equal); Investigation (equal); Validation (equal); Writing—review and editing (equal). **Luca Stendardo:** Conceptualization (equal); Funding acquisition (lead); Project administration (equal); Validation (equal); Writing—review and editing (equal). **Younes Rafik:** Investigation (supporting); Methodology (supporting). **Jason Pothin:** Investigation (supporting); Methodology (supporting). **Marc Budinger:** Investigation (supporting); Methodology (supporting); Validation (equal). **Carlo Antonini:** Conceptualization (equal); Funding acquisition (lead); Project administration (equal); Validation (equal); Writing—review and editing (equal). **Valérie Pommier-Budinger:** Conceptualization (equal); Validation (equal); Writing—review and editing (equal). **Anna Maria Coclite:** Conceptualization (equal); Funding acquisition (equal); Project administration (equal); Supervision (lead); Validation (equal); Writing—review and editing (equal).

Data Availability Statement

The data that support the findings of this study are available from the corresponding author upon reasonable request.

Keywords

anti-icing systems initiated chemical vapor deposition, electromechanical de-icing systems, hybrid de-icing systems, icephobic, icing wind tunnel, polymer coatings

- [1] H. Sojoudi, M. Wang, N. D. Boscher, G. H. McKinley, K. K. Gleason, *Soft Matter* **2016**, *12*, 1938.
- [2] X. Huang, N. Tepylo, V. Pommier-Budinger, M. Budinger, E. Bonaccorso, Villedieu, L. Bennani, *Prog. Aerosp. Sci.* **2019**, *105*, 74.
- [3] Z. He, C. Wu, M. Hua, S. Wu, D. Wu, X. Zhu, J. Wang, X. He, *Matter* **2020**, *2*, 723.
- [4] K. Golovin, S. R. Kobaku, D. H. Lee, E. T. Diloireto, J. M. Mabry, A. Tuteja, *Sci. Adv.* **2016**, *2*, e1501496.
- [5] Q. Guo, Z. He, Y. Jin, S. Zhang, S. Wu, G. Bai, H. Xue, Z. Liu, S. Jin, L. Zhao, J. Wang, *Langmuir* **2018**, *34*, 11986.
- [6] L. Snels, N. Mostofi Sarkari, J. Soete, A. Maes, C. Antonini, M. Wevers, T. Maitra, D. Seveno, *J. Colloid Interface Sci.* **2023**, *637*, 500.
- [7] M. J. Tavaststjerna, S. J. Picken, S. J. Garcia, *Langmuir* **2024**, *40*, 12888.
- [8] W. Li, Y. Zhan, S. Yu, *Prog. Org. Coat.* **2021**, *152*, 106117.
- [9] W. Huang, J. Huang, Z. Guo, W. Liu, *Adv. Colloid Interface Sci.* **2022**, *304*, 102658.
- [10] R. Rekuviene, S. Saeidharzand, L. Mažeika, V. Samaitis, A. Jankauskas, A. K. Sadaghiani, G. Gharib, Z. Muganli, A. Koşar, *Appl. Therm. Eng.* **2024**, *250*, 123474.
- [11] Z. He, H. Xie, M. I. Jamil, T. Li, Q. Zhang, *Adv. Mater. Interfaces* **2022**, *9*, 2200275.
- [12] X. Guo, Q. Yang, H. Zheng, W. Dong, *Appl. Therm. Eng.* **2024**, *236*, 121723.
- [13] Z. Zhao, Y. Wang, Z. Wang, X. Cui, G. Liu, Y. Zhang, Y. Zhu, J. Chen, S. Sun, K. Zhang, X. Liu, H. Chen, *Small* **2024**, *20*, 2311435.
- [14] P. Pellicano, J. Riley, in *45th AIAA Aerospace Sciences Meeting and Exhibit*, American Institute of Aeronautics and Astronautics, Reston, Virginia, January **2007**, <https://doi.org/10.2514/6.2007-1090>.
- [15] L. Chen, X. Ni, Y. Zhou, Y. Shen, L. Qian, *Polym. Test.* **2024**, *133*, 108405.
- [16] X. Li, Y. Liu, J. Leng, *Sustainable Mater. Technol.* **2023**, *37*, e00692.
- [17] L. Ding, X. Wang, W. Zhang, S. Wang, J. Zhao, Y. Li, *Appl. Sci.* **2018**, *8*, 2360.
- [18] V. Palanque, J. Pothin, V. Pommier-Budinger, M. Budinger, *Chin. J. Aeronaut.* **2024**, *37*, 92.
- [19] G. Fortin, M. Adomou, J. Perron, SAE Technical Paper 2011-38-0003, **2011**. <https://doi.org/10.4271/2011-38-0003>.
- [20] C. Antonini, M. Innocenti, T. Horn, M. Marengo, A. Amirfazli, *Cold Reg. Sci. Technol.* **2011**, *67*, 58.
- [21] M. Budinger, V. Pommier-Budinger, A. Reysset, V. Palanque, *AIAA J.* **2021**, *59*, 2590.
- [22] S. V. Venna, Y.-J. Lin, G. Botura, *J. Aircr.* **2007**, *44*, 509.
- [23] V. Pommier-Budinger, M. Budinger, Rousset, F. Dezitter, F. Huet, M. Wetterwald, E. Bonaccorso, *AIAA J.* **2018**, *56*, 4400.
- [24] G. Gastaldo, M. Budinger, Y. Rafik, V. Pommier-Budinger, V. Palanque, A. Yaich, *Ultrasonics* **2024**, *138*, 107264.
- [25] V. Palanque, T. Planès, -B. Valérie, B. Marc, D. Scott, *Chin. J. Aeronaut.* **2024**, *37*, 50.
- [26] G. Hernández Rodríguez, M. Fratschko, L. Stendardo, C. Antonini, R. Resel, A. M. Coclite, *ACS Appl. Mater. Interfaces* **2024**, *16*, 11901.
- [27] A. M. Coclite, Y. Shi, K. K. Gleason, *Adv. Funct. Mater.* **2012**, *22*, 2167.
- [28] K. K. S. Lau, K. K. Gleason, *Macromolecules* **2006**, *39*, 3688.
- [29] L. Stendardo, G. Gastaldo, M. Budinger, V. Pommier-Budinger, I. Tagliaro, F. Ibáñez-Ibáñez, C. Antonini, *Appl. Surf. Sci.* **2023**, *641*, 158462.

- [30] L. Stendardo, G. Gastaldo, M. Budinger, C. Antonini, V. Pommier-Budinger, and A. C. Ospina Patiño, SAE Technical Paper 2023-01-1451, **2023**, <https://doi.org/10.4271/2023-01-1451>.
- [31] K. Golovin, A. Dhyani, M. D. Thouless, A. Tuteja, *Science* **2019**, 364, 371.
- [32] K. K. Gleason, *Adv. Mater.* **2024**, 36, 2306665.
- [33] K. Unger, A. M. Coclite, *Pharmaceutics* **2020**, 12, 904.
- [34] H. Memon, J. Wang, X. Hou, *Materials* **2023**, 16, 4607.
- [35] K. Maghsoudi, E. Vazirinasab, G. Momen, R. Jafari, *J. Mater. Process. Technol.* **2021**, 288, 116883.
- [36] H. Memon, J. Liu, D. S. A. De Focatiis, K. Choi, X. Hou, *Surf. Coat. Technol.* **2020**, 385, 125382.
- [37] S. Schröder, O. Polonskyi, T. Strunskus, F. Faupel, *Mater. Today* **2020**, 37, 35.